

A single-shot measurement of time-dependent diffusion over sub-millisecond timescales using static field gradient NMR

Teddy X. Cai,^{1,2} Nathan H. Williamson,^{1,3} Velencia J. Witherspoon,¹ Rea Ravin,^{1,4} and Peter J. Basser^{1, a)}

¹⁾ *Section on Quantitative Imaging and Tissue Sciences, Eunice Kennedy Shriver National Institute of Child Health and Human Development, National Institutes of Health, Bethesda, Maryland 20892, USA*

²⁾ *Wellcome Centre for Integrative Neuroimaging, Nuffield Department of Clinical Neurosciences, University of Oxford, Oxford, UK*

³⁾ *National Institute of General Medical Sciences, National Institutes of Health, Bethesda, Maryland 20892, USA*

⁴⁾ *Celoptics, Rockville, Maryland 20852, USA*

(Dated: 29 December 2020)

Time-dependent diffusion behavior is probed over sub-millisecond timescales in a single shot using an NMR static gradient, time-incremented echo train acquisition (SG-TIETA) framework. The method extends the Carr-Purcell-Meiboom-Gill (CPMG) cycle under a static field gradient by discretely incrementing the π -pulse spacings to simultaneously avoid off-resonance effects and probe a range of timescales (50 – 500 μ s). Pulse spacings are optimized based on a derived ruleset. The remaining effects of pulse inaccuracy are examined and found to be consistent across pure liquids of different diffusivities: water, decane, and octanol-1. A pulse accuracy correction is developed. Instantaneous diffusivity, $D_{\text{inst}}(t)$, curves (i.e., half of the time derivative of the mean-squared displacement in the gradient direction), are recovered from pulse accuracy-corrected SG-TIETA decays using a model-free, log-linear least squares inversion method validated by Monte Carlo simulations. A signal-averaged, 1-minute experiment is described. A flat $D_{\text{inst}}(t)$ is measured on pure dodecamethylcyclohexasiloxane whereas decreasing $D_{\text{inst}}(t)$ are measured on yeast suspensions, consistent with the expected short-time $D_{\text{inst}}(t)$ behavior for confining microstructural barriers on the order of microns.

I. INTRODUCTION

As molecules diffuse, they interact with their surroundings and “[feel] the boundary”¹, causing their ensemble displacement behavior to be influenced by the morphology of the microenvironment. More specifically, long-range correlations such as confining barriers impart a nonlinear time-dependence to the ensemble-averaged net mean-squared displacement, $\langle \mathbf{r}^2(t) \rangle$ (in \mathbb{R}^3). This leads to a time-dependent diffusion coefficient^{2,3},

$$D(t) = \frac{\langle \mathbf{r}^2(t) \rangle}{6t} \equiv \frac{1}{3t} \int_0^t (t-t') \text{tr}(\mathcal{D}(t')) dt', \quad (1)$$

where $\mathcal{D}(t') = H(t') \langle \mathbf{v}(t') \mathbf{v}^T(0) \rangle \equiv \partial_t^2 [H(t) \langle \mathbf{r}(t) \mathbf{r}^T(0) \rangle]$ is the causal velocity autocorrelation tensor, $H(t)$ is the unit step function, and “tr” is the trace operation.

Microstructural features can be inferred from the behavior of $D(t)$ at limiting short and long timescales (see Sen⁴ and Reynaud⁵ for review). At the short-time limit, $D(t)$ exhibits universal behavior² which depends on the barrier surface-to-volume ratio, S/V ,

$$D(t) \simeq D_0 \left[1 - \frac{S}{V} \left(\frac{4\ell_D}{9\sqrt{\pi}} \right) \right], \quad t \rightarrow 0, \quad (2)$$

where $\ell_D = \sqrt{D_0 t}$ is the diffusion length scale and $D_0 \equiv D(t)|_{t=0}$ is the free diffusivity. As ℓ_D increases,

the barrier permeability, κ , may begin to affect $D(t)$ ⁶⁻⁹. While ℓ_D remains short, barriers appear flat to the small fraction of nearby walkers that encounter them^{8,10}, introducing a linear κt term in Eq. (2),

$$D(t) \simeq D_0 \left[1 - \frac{S}{V} \left(\frac{4\ell_D}{9\sqrt{\pi}} - \kappa t \right) \right], \quad t \ll \tau_D, \quad (3)$$

where $\tau_D = \bar{a}^2/(2D_0)$ is the time to diffuse across the mean pore of size $\bar{a} = 6V/S$. Curvature⁸ and surface-relaxivity³ may also affect $D(t)$. Tortuosity principally affects the long-time $D(t)$ ^{11,12} and can be categorized into disorder classes with structural exponent, p ^{10,13}. The long-time $D(t)$ follows a p -dependent power law¹³,

$$D(t) \simeq D_\infty + \text{const.} \cdot t^{-\vartheta}, \quad t \rightarrow \infty, \quad (4)$$

where $D_\infty = \lim_{t \rightarrow \infty} D(t)$ and $\vartheta = (p+3)/2$.

Diffusion-weighted (DW) nuclear magnetic resonance (NMR) methods are highly sensitive to $\langle \mathbf{r}^2(t) \rangle$ ¹⁴⁻²⁰, and provide a powerful means to probe rich $D(t)$ behaviors and infer distinct microstructural features. DW-NMR experiments have been used to study the short- and long-time $D(t)$ in porous media ranging from sedimentary rock to skeletal muscle^{5,12,13,21-25}.

The NMR spin echo dephasing, however, is not simply written in terms of $D(t)$ itself. Instead, the echo dephasing is often expressed in terms of the real part, \Re , of the Fourier transform of $\mathcal{D}(t)$ ²⁶⁻²⁸. From Eq. (1)²⁸,

$$\frac{\text{tr}(\Re[\mathcal{D}(\omega)])}{3} = D_0 + \int_0^\infty \partial_t^2 [tD(t)] e^{i\omega t} dt. \quad (5)$$

^{a)} Electronic mail: peter.basser@nih.gov

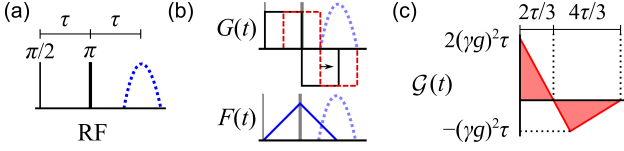


FIG. 1. Example $\mathcal{G}(t)$ calculation. (a) Radiofrequency (RF) pulses in a static gradient of amplitude g . (b) $G(t)$, shifted $G(t+s)$ (red, dashed), and $F(t)$. (c) Corresponding $\mathcal{G}(t)$.

High and low frequency $\text{tr}(\Re[\mathcal{D}(\omega)])$ behaviors reveal the short- and long-time $D(t)$, respectively. The relationship between $\Re[\mathcal{D}(\omega)]$ and the ensemble echo dephasing follows from a cumulant expansion of the phase expectation value and a Gaussian phase distribution approximation²⁹, yielding the normalized echo intensity^{30,31},

$$\frac{I(T)}{I_0} = \exp\left(-\frac{1}{\pi} \int_0^\infty \mathbf{F}^T(\omega) \Re[\mathcal{D}(\omega)] \mathbf{F}(\omega) d\omega\right), \quad (6)$$

where $\mathbf{F}(\omega)$ is the truncated Fourier transform of $\mathbf{F}(t)$ at the echo time (i.e., $\mathbf{F}(T) = \mathbf{0}$),

$$\mathbf{F}(\omega) = \int_0^T \mathbf{F}(t) e^{i\omega t} dt, \quad (7)$$

$\mathbf{F}(t) = \gamma \int_0^t \mathbf{G}(t') dt'$, $\mathbf{G}(t)$ is the gradient waveform, and γ is the gyromagnetic ratio. The assumed Gaussian phase approximation is valid for most relevant experimental cases^{32,33} (cf. Stepišnik³⁴).

Eqs. (6) and (7) show that spectral tuning of $|\mathbf{F}(\omega)|^2$ results in narrow sampling of $\Re[\mathcal{D}(\omega)]$ in the gradient direction, $\hat{\mathbf{g}}$. $\mathbf{G}(t)$ can be periodically time-modulated³⁵ (e.g., by using a sinusoidal $\mathbf{G}(t)$ ²⁴) so that the spectral density of $|\mathbf{F}(\omega)|^2$ concentrates near some frequency, ω_F . In this case, $I(T)/I_0$ becomes well-approximated by $\exp(-b(T) \times \hat{\mathbf{g}}^T \Re[\mathcal{D}(\omega_F)] \hat{\mathbf{g}})$, where¹⁶

$$b(T) = \int_0^T |\mathbf{F}(t)|^2 dt \equiv \frac{1}{\pi} \int_0^\infty |\mathbf{F}(\omega, T)|^2 d\omega. \quad (8)$$

Individual experiments become a point-wise sampling of $\hat{\mathbf{g}}^T \Re[\mathcal{D}(\omega_F)] \hat{\mathbf{g}}$. This “temporal diffusion spectroscopy”³⁶ approach is robust, but has limited time resolution because it individually probes ω_F . Furthermore, the shortest probe-able timescale (i.e., largest ω_F) is limited to about 10 ms by the pulsed gradient hardware^{5,36}. An alternative approach is needed for the real-time study of $D(t)$ across timescales and to reach the information-rich, short-time regime ($\lesssim 1$ ms) in biological systems.

II. THEORY

A. Time-dependent signal representation

To begin, an alternative signal representation is used. The echo attenuation is related to the stationary position autocorrelation tensor, $\mathcal{R}(t, t') =$

$\langle \mathbf{r}(t) \mathbf{r}^T(t') \rangle \equiv \mathcal{R}(|t - t'|)$ – again assuming a Gaussian phase distribution^{30,31,37} – by

$$\frac{I(T)}{I_0} = \exp\left(-\frac{\gamma^2}{2} \int_0^T \int_0^T \mathbf{G}^T(t) \mathcal{R}(t, t') \mathbf{G}(t') dt dt'\right), \quad (9)$$

Eq. (9) can be rewritten according to Ning et al.³⁷ by integrating along the level set of $t - t'$. For unidirectional encoding, i.e., $G(t) = \|\mathbf{G}(t)\|$ and $F(t) = \gamma \int_0^t G(t') dt'$,

$$\frac{I(T)}{I_0} = \exp\left(-\int_0^T \mathcal{C}(t) D_{\text{inst}}(t) dt\right), \quad (10)$$

where $D_{\text{inst}}(t)$ is the *instantaneous* diffusivity along the gradient direction $\hat{\mathbf{g}}$,

$$D_{\text{inst}}(t) := \partial_t \left[\frac{\hat{\mathbf{g}}^T \mathcal{R}(t) \hat{\mathbf{g}}}{2} \right] \equiv \partial_t \left[\frac{\langle [\mathbf{r}(t) \cdot \hat{\mathbf{g}}]^2 \rangle}{2} \right], \quad t > 0, \quad (11)$$

(dropping $\hat{\mathbf{g}}$ as implied) and $\mathcal{C}(t)$ is the cumulative integral of the $\gamma G(t)$ autocorrelation function,

$$\begin{aligned} \mathcal{C}(t) &= \int_0^t \mathcal{G}(t') dt', \\ \mathcal{G}(t') &= \gamma^2 \int_0^{t'} G(t'') G(t'' + s) ds \end{aligned} \quad (12)$$

schematized in Fig. 1. The attenuation becomes a sampling of $D_{\text{inst}}(t)$ weighted by $\mathcal{C}(t)$, similar to how Eq. (6) describes a sampling of $\Re[\mathcal{D}(\omega)]$ by $|\mathbf{F}(\omega)|^2$.

B. Recasting the problem

Eq. (10) is advantageous compared to Eq. (6) because $\mathcal{C}(t)$ is simple for general, non-periodic $G(t)$. The ill-posed inverse problem of finding $D_{\text{inst}}(t)$ from many trivial $G(t)$ is tractable. For a train of N echoes refocusing at times T_n , $\mathcal{C}_n(t)$ can be evaluated for each inter-echo attenuation, i.e., $I(T_n)/I(T_{n-1})$ ($T_0 = 0$). By discretizing the time domain into K bins of variable width, $\Delta t(k)$, the problem can be cast into a weighted and regularized log-linear least squares (LLS) form:

$$\arg \min_{\mathbf{X}} \|\mathbf{W}^{1/2} (\mathbf{A}\mathbf{X} - \mathbf{B})\|_2^2 + \lambda \|\Gamma \mathbf{X}\|_2^2, \quad (13)$$

with coefficients

$$\mathbf{A} = \begin{bmatrix} \int_0^{\Delta t(1)} \mathcal{C}_1(t) dt & \dots & \int_{\Delta t(K-1)}^{\Delta t(K)} \mathcal{C}_1(t) dt \\ \vdots & & \vdots \\ \int_0^{\Delta t(1)} \mathcal{C}_N(t) dt & \dots & \int_{\Delta t(K-1)}^{\Delta t(K)} \mathcal{C}_N(t) dt \end{bmatrix},$$

where \mathbf{X} consists of time-interval $D_{\text{inst}}(t)$ averages,

$$\mathbf{X} = \begin{bmatrix} \frac{1}{\Delta t(1)} \int_0^{\Delta t(1)} D_{\text{inst}}(t) dt \\ \vdots \\ \frac{1}{\Delta t(K) - \Delta t(K-1)} \int_{\Delta t(K-1)}^{\Delta t(K)} D_{\text{inst}}(t) dt \end{bmatrix},$$

and $\mathbf{B}^T = -\ln [I(T_1)/I_0 \dots I(T_N)/I(T_{N-1})]$. The regularization matrix, $\mathbf{\Gamma}$, is chosen to consist of first and second-order finite difference matrices, reflecting an *a priori* assumption of the smoothness and concavity of $D_{\text{inst}}(t)$. The norm is weighted by a proportionality of the signal-to-noise ratio (SNR); since \mathbf{B} consists of log ratios, the appropriate weights matrix, \mathbf{W} , is an $N \times N$ matrix of signal differences, i.e., $I(T_{n-1}) - I(T_n)$. In this way, $D_{\text{inst}}(t)$ can be estimated from a single echo train with varied $C_n(t)$.

We arrive at the motivating question of this Communication: Can a DW-NMR method probe the time-varying diffusivity in real-time? With Eq. (13) in mind, the question can be separated into two parts: (1) How can $C_n(t)$ of various time sensitivities be produced in one echo train? (2) How can every echo be made accurate? The answer to the first part follows from a well-known DW-NMR protocol. A Carr-Purcell-Meiboom-Gill (CPMG)^{38,39} π -pulse train under an SG in the radiofrequency (RF) field produces a triangle wave $F(t)$ with $\omega_F = (\pi/2\tau)$ rad/s, where 2τ is the spacing between π -pulses. This SG-CPMG ω_F (up to tens of kHz²³) far exceeds that which is attainable with oscillating or pulsed field gradient (PFG) methods (~ 100 Hz). Indeed, the SG-CPMG method is uniquely capable of probing the short-time diffusion regime in small ($\bar{a} \lesssim \mu\text{m}$) structures^{23,35,40-43}.

Varying the π -pulse spacing in an SG-CPMG-type acquisition is therefore the best method to produce many varied $C_n(t)$ in one shot. Spacings might be incremented to retain signal. We choose the spacing between π -pulses to take the form: $2\tau + m_j\delta$, where j indexes the π -pulse-to-pulse spacing, $m_j \in \mathbb{N}$, and δ is a unit time increment. We term this discrete spacing method the SG, time-incremented echo train acquisition (SG-TIETA), e.g., Fig. 2. For SG-TIETA,

$$C_n(t) = \gamma^2 g^2 \begin{cases} t(-\frac{3}{2}t + 2h_n) & 0 \leq t \leq h_n \\ t(\frac{1}{2}t - h_n) + 2h_n^2 & h_n \leq t \leq 2h_n \end{cases}, \quad (14)$$

where h_n is the n th peak of $|F(t)|/\gamma g$.

C. Avoiding off-resonance signal contributions

Ignoring magnetic susceptibility, spin-spin (T_2) relaxation, and surface-relaxivity³ effects, the predominant source of extraneous signal decay is off-resonance coherence transfer pathways (CTPs). When the bandwidth of Larmor precession frequencies spanned by an SG exceeds the bandwidth of π -pulses, every pulse is slice-selective and excites all CTPs²⁰. For SG-CPMG measurements, the number of refocused off-resonance CTPs grows exponentially with N ($\sim 3^{N44}$), resulting in significant deviations from the expected echo attenuation⁴⁴⁻⁴⁷. Phase cycling remediation schemes require $\sim 2^N$ steps⁴⁸ and are thus infeasible. Unconventional approaches such as time-based avoidance of CTPs^{49,50} become necessary. An SG aids these time-based approaches by acting as an always-on crusher gradient. The minimum time separation to

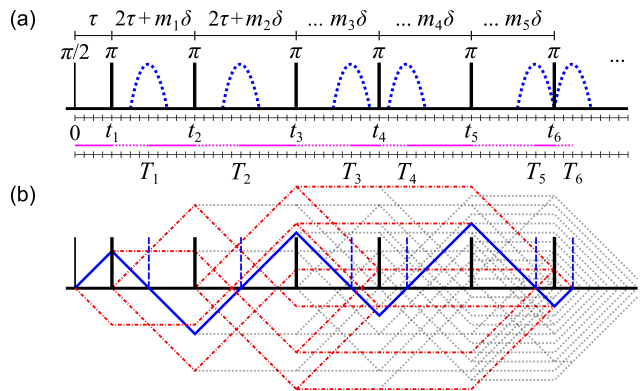


FIG. 2. Example SG-TIETA sequence. (a) Timings: $m_j = \{1, 3, 1, 2, 1\}$, $\tau = 4\delta$, and $\delta = 14 \mu\text{s} = 1$ dash. π -pulses occur at t_n and echoes form at T_n . Magenta line indicates timing behavior: $T_n = t_n + h_n$, where h_n is the normalized $|F(t)|/\gamma g$ “height” at t_n , given by $h_1 = \tau$ and $h_n = 2\tau + m_n\delta - h_{n-1}$ for $n > 1$. (b) Direct echo $F(t)$ and other coherence pathways that refocus (red, dash-dot) or do not refocus (gray, dotted).

avoid undesired signal, τ_{sep} , is shortened. Specifically, τ_{sep} is constrained by $\tau_{\text{sep}} \geq \tau_p$, where $\tau_p = 2\pi/(\gamma g \Delta z)$ is the length of the π -pulse and Δz is the resulting slice thickness. The echo width under an SG is on the order of τ_p ⁵¹ such that this constraint can be understood as avoiding undesired echo overlap. For hard π -pulses, $\tau_p \sim \mu\text{s}$.

We should thus ask: What choice of m_j , τ , and δ separates off-resonance CTPs from the direct echo CTP by $\geq \tau_p$? Consider that CTPs are piece-wise linear functions in $F(t)$. The three magnetization states for a spin-1/2 nuclei (in shorthand: $M \in \{+, -, 0\}$ ⁴⁷) correspond to $+\gamma G$, $-\gamma G$, and 0 slopes, respectively (see Fig. 2b). Refocusing of undesired signal occurs when the summed difference between an off-resonance $F(t)$ and the direct echo $F(t)$, $\sum \Delta F(t)$, equals 0. Rules for m_j , τ , and δ are developed. Singly stimulated echoes (e.g., $+0-$) arise due to two h_n matching. Thus:

- (i) Absolute $F(t)$ heights, or h_n , may not be repeated.

Next, consider CTPs that see the initial $\pi/2$ -pulse. These CTPs can alter $\sum \Delta F(t)/\gamma g$ by one of $\{0, 1, 2\} \times (-1)^{j-1}(2\tau + m_j\delta)$. Accounting for $\sum \Delta F(t) = 0$ with up to four non-zero terms:

- (ii) m_j and $m_{j \pm \Delta j}$ with odd Δj may not be the same.
- (iii) Twice any m_j may not equal the sum of $m_{j+\Delta j}$ and $m_{j-\Delta j}$ for even Δj .
- (iv) Any two m_j with even j may not equal the sum of any two m_j with odd j .
- (v) Twice any m_j with even j may not equal the sum of any two m_j with odd j , and vice versa.

Off-resonance CTPs also arise from the introduction of signal via effective $\pi/2$ -pulses. These CTPs invariably

start with $\sum \Delta F(t)$ containing an odd multiple of τ (i.e., $\tau + 2j\tau$). Choosing τ and δ such that $(\tau \bmod \delta) = \delta/2$ thus ensures that $\sum \Delta F(t) \geq \delta/2$. Incorporating τ_p :

(vi) δ and τ satisfy $(\tau \bmod \delta) = \delta/2$ and $\delta > 2\tau_p$.

Note that $(\tau \bmod \delta) = 0$ results in the refocused CTPs in Fig. 2b. This limited ruleset (i–vi) may be sufficient to ostensibly avoid off-resonance effects considering that singly stimulated echoes are known to be the most significant contributor to SG-CPMG off-resonance effects^{44,47}.

The generation of m_j that satisfies rules (i–v) is discussed in the Supplementary Material (SM) Section I. Python code is provided. A solution for τ , δ , and m_j that probes t from $\sim 50 - 500 \mu\text{s}$ is

$$\tau = 49 \mu\text{s}, \quad \delta = 14 \mu\text{s},$$

$$m_j = \left\{ \begin{array}{cccccccccccc} 1 & 3 & 6 & 7 & 10 & 12 & 11 & 15 & 20 & 21 \\ 24 & 26 & 20 & 21 & 33 & 35 & 33 & 34 & 33 & \dots \end{array} \right\}. \quad (15)$$

This timing sequence is used throughout.

III. EXPERIMENTAL SETUP

NMR measurements were performed at $\mathbf{B}_0 = 0.3239 \text{ T}$ (proton $\omega_0 = 13.79 \text{ MHz}$) using a PM-10 NMR MOUSE single-sided permanent magnet⁵² (Magritek, Aachen Germany) and a Kea 2 spectrometer (Magritek, Wellington, New Zealand). The decay of the magnetic field with distance from the magnet produces a strong $g = 15.3 \text{ T/m}$ (650 kHz/mm) static gradient. Measurements used a home-built test chamber and a $13 \times 2 \text{ mm}$ solenoid RF coil and RF circuit. Additional information concerning the experimental setup can be found in Williamson et al.⁵³. The SG-TIETA pulse program was written in Prospa V3.22, modified from the standard CPMG sequence. See SM Section IV for further details.

For measurements on twice-distilled water, decane (Sigma-Aldrich, St. Louis, MO, USA.), 1-octanol (Sigma-Aldrich), and dodecamethylcyclohexasiloxane (D6) kinematic Viscosity = 6.6 cSt @ 25°C (Gelest, inc. Morrisville, PA, USA.), the liquids were transferred to 2 cm glass capillary sections (1.1 mm OD, Kwik-Fil™, World Precision Instruments, Inc., Sarasota, FL, USA) and the capillaries were sealed with a hot glue gun.

For measurements on yeast (*S. cerevisiae*), 1.72 g of dry yeast was mixed in 10 ml of tap water and stored in a 50 ml tube with the lid screwed on loosely to allow gas to escape. After three days (72 h), the yeast was re-suspended and samples were taken for NMR experiments and for cell density measurement. The cell density of the first sample (yeast #1) was measured to be $2.84 \times 10^9 \text{ cells/ml}$ using a hemocytometer. The remaining yeast was centrifuged, the pellet was re-diluted to 2X the initial concentration, and a second sample (yeast #2) was taken for NMR experiments. Immediately prior to experiments, yeast was transferred to 2 cm KrosFlow® Implant Membrane sections (500,000 Dalton molecular

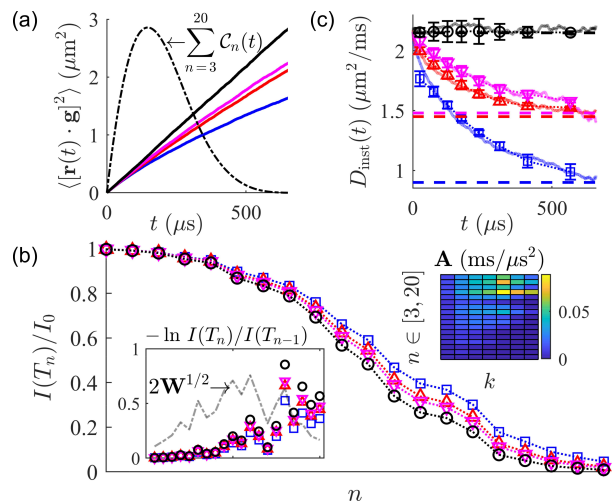


FIG. 3. LLS inversion on Monte Carlo simulated data. (a) Simulated $\langle |\mathbf{r}(t) \cdot \hat{\mathbf{g}}|^2 \rangle$ ($D_0 = 2.15 \mu\text{m}^2/\text{ms}$) for free diffusion (black) and restricted geometries (see Fig. S1). $\sum C_n(t)$ (a.u.) for Eq. (15) is overlaid, omitting the first two echoes. (b) Simulated decays ($\gamma g = 4.093 \mu\text{m}^{-1}\text{ms}^{-1}$) from same color curves in (a). Insets show \mathbf{B} with $2\mathbf{W}^{1/2}$ for free diffusion and \mathbf{A} for $\Delta t(k) = \{50, 50, 50, 50, 75, 75, 125, 139\} \mu\text{s}$. (c) $D_{\text{inst}}(t)$ from gradient of $\langle |\mathbf{r}(t) \cdot \hat{\mathbf{g}}|^2 \rangle$ curves in (a) (solid lines) compared to \mathbf{X} inverted from decays in (b) with added Gaussian noise (SNR = 25). Err. bars = ± 1 SD from 100 replications. Initial \mathbf{X} guesses were D_0 for the first point and D_∞ (dashed lines, $\{0.9, 1.45, 1.48\} \mu\text{m}^2/\text{ms}$) for remaining points. $\lambda = 2 \times 10^{-6}$, selected manually. See Eq. (S1) for $\mathbf{\Gamma}$.

weight cut off, 1 mm OD, SpectrumLabs, Waltham, MA, USA) and the membranes were sealed by pinching the membrane with heated forceps. Yeast was kept from drying out by performing measurements immediately upon filling and sealing the capillary and by lining the inside with wet tissue paper to increase humidity.

Experiments were performed at ambient temperature. Sample temperature was monitored with a fiber optic sensor (PicoM Opsens Solutions Inc., Québec, Canada). The average temperatures of the samples during the course of the experiments were 25°C, 22°C, 22°C, 23°C, and 24°C for the water, decane, octanol-1, D6, and yeast.

IV. RESULTS AND DISCUSSION

As an initial proof-of-principle, the LLS inversion described in Eq. (13) is demonstrated in Fig. 3 on noisy SG-TIETA decays generated using the timings in Eq. (15) and $\langle |\mathbf{r}(t) \cdot \hat{\mathbf{g}}|^2 \rangle$ curves from Monte Carlo simulations⁵⁴. Further details and MATLAB code are provided in SM Section II. Inverted \mathbf{X} values are accurate and robust to noise. No systematic errors other than potential over-regularization (e.g., blue curve, Fig. 3c) are observed.

Echo-to-echo accuracy remains experimentally difficult to achieve, however. Consider the signal decay due to

T_2 relaxation and pulse inaccuracy effects⁴⁷. Relaxation may be ignored if $(2\tau + m_j\delta) \ll T_2 \forall j$. Diffusion-weighted T_2 values for each sample, as shown in Table I, indicate that this condition holds for all pure liquids studied here. However, the yeast is described by a distribution of T_2 with a 5% water population with T_2 similar to $\max\{2\tau + m_j\delta\} = 539 \mu\text{s}$. The instantaneous diffusion measurements of yeast may be slightly weighted by T_2 relaxation. See SM Section IV for relaxation measurement methods and yeast #2 T_2 distribution analysis. Unlike T_2 , pulse inaccuracy cannot be ignored. Inaccuracy effects may be described using an n -dependent pulse accuracy factor, $A_p(n)$ ⁴⁷. The signal is then corrected as $I(T_n)/I_0 \times [1/\prod_{l=1}^n A_p(l)]$, assuming total avoidance of off-resonance CTPs via rules (i-vi).

TABLE I. Relaxation times.

Sample	T_1 [ms]	T_2 [ms]
water	3250	133
decane	1340	166
octanol-1	440	217
D6	788	292
yeast #1 (2.84B cells/mL)	625	59
yeast #2 (5.68B cells/mL)	319	41

Calibration $A_p(n)$ values were approximated from decays of pure liquids, shown in Fig. 4. A 16 μs echo window was used. All decays were normalized to the first echo and each repetition consisted of 32 summed (i.e., signal-averaged) scans. To better understand the expected $A_p(n)$ behavior, we consider the spatial, i.e., slice effects. The bandwidth or slice excited by refocusing π -pulses has inconsistent frequency content^{55,56} such that $A_p(n) < 1$. With each pulse, spins which rotate by angles other than π do not refocus until only a stable, central slice remains. In the time domain, this slice-thinning and loss of frequency content is expected to broaden the echo width, which we experimentally verify in Fig. 5. Based on the evolution of the echo shape, $A_p(n)$ should sharply increase then taper. This behavior is observed in Fig. 4c and is consistent across liquids of vastly different D_0 . Similar $A_p(n)$ values were also obtained for $\tau = 77 \mu\text{s}$ (see SM Section III, Fig. S5), further supporting that $A_p(n)$ is independent of the diffusion weighting.

Another pre-processing step is designed to mitigate the effects of early $A_p(n)$ variability and to ensure the non-negativity of \mathbf{B} and \mathbf{W} entries. A piece-wise linear fit of adjacent $\ln(I(T_n)/I_0)$ points vs. b is performed, specifying (1) an intercept with $[b, \ln(I(T_n)/I_0)] = [0, 0]$, (2) no slope exceeds D_0 , and (3) the piece-wise slopes decrease monotonically (i.e., $D_{\text{inst}}(t)$ has non-negative concavity). Altogether, SG-TIETA decays are analyzed in five steps: (1) summing 32 \times , (2) normalization to the first echo, (3) $I(T_n)/I_0 \times [1/\prod_{l=1}^n A_p(l)]$ correction, (4) a constrained log- b domain fit to the repetition(s), and, finally, (5) the LLS inversion. This pipeline was applied to SG-TIETA

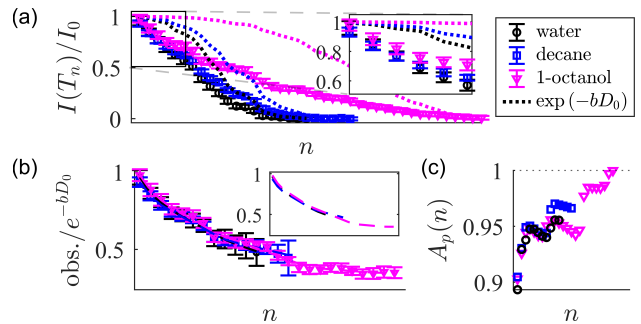


FIG. 4. SG-TIETA $A_p(n)$ calibration using pure liquids. (a) Observed SG-TIETA decays compared to $\exp(-bD_0)$. D_0 was measured (see SM Section IV) in legend order as 2.22 ± 0.01 , 1.27 ± 0.01 , $0.121 \pm 0.002 \mu\text{m}^2/\text{ms}$. Err. bars = ± 1 SD for 25, 38, 70 repetitions, respectively. (b) Decay vs. $\exp(-bD_0)$ ratio truncated at $n = 12, 15, 25$. Inset shows cubic spline fits. (c) $A_p(n)$ approximated using adjacent fitted ratios.

decays of D6 and yeast using the 1-octanol and water $A_p(n)$ values obtained in Fig. 4c, respectively.

Results are summarized in Fig. 6. The $D_{\text{inst}}(t)$ for D6 – with $D_0 = 0.114 \pm 0.008 \mu\text{m}^2/\text{ms}$ – is expectedly flat, thus validating the $A_p(n)$ correction. The $D_{\text{inst}}(t)$ for yeast are the key results of this Communication. For comparison, the short-time $D_{\text{inst}}(t)$ predicted by Eq. (3) (i.e., $d[tD(t)]/dt$) is plotted for several S/V and κ values. Fig. 6b indicates that $\bar{a} \simeq 2 \mu\text{m}$ and that a doubling of the cell density approximately halves \bar{a} . For yeast's $\approx 4 \mu\text{m}$ spherical diameter⁵⁷, \bar{a} is calculated as 42 and 21 μm at these cell densities, suggesting contributions from sub-cellular length scales. This ensemble \bar{a} estimate of $\simeq 2 \mu\text{m}$ ($\equiv V/S \simeq 3 \mu\text{m}$) is within the range of estimates ($\bar{a} \sim 1 - 5 \mu\text{m}$) reported in previous PFG and SG DW-NMR studies of similar yeast densities⁵⁷⁻⁶¹. These yeast results are considered non-quantitative, however, due to T_2 contributions, the Gaussian phase approximation, and the stationary $\hat{\mathbf{g}}^T \mathcal{R}(t, t') \hat{\mathbf{g}}$ assumption. Heterogeneous microenvironments result in progressive signal weighting towards less mobile spins and thus violate inter-echo stationarity. Indeed, heterogeneity may explain the convergence of the yeast $D_{\text{inst}}(t)$. Nonetheless, the sensitivity of SG-TIETA to *apparent* microstructural features is clear.

V. CONCLUSIONS

We have developed a real-time protocol to measure time-varying diffusion. Inversion for $D_{\text{inst}}(t)$ from experimental SG-TIETA decays is demonstrated. A $\simeq 1$ -minute (32 \times repetition time of 2 s) experiment is described. In contrast to conventional temporal diffusion spectroscopy methods, the single-shot nature of SG-TIETA permits true signal averaging in order to improve SNR. A *post hoc* $A_p(n)$ correction is proposed to improve the quantitative accuracy of the method. To support the validity of this correction, we present preliminary evi-

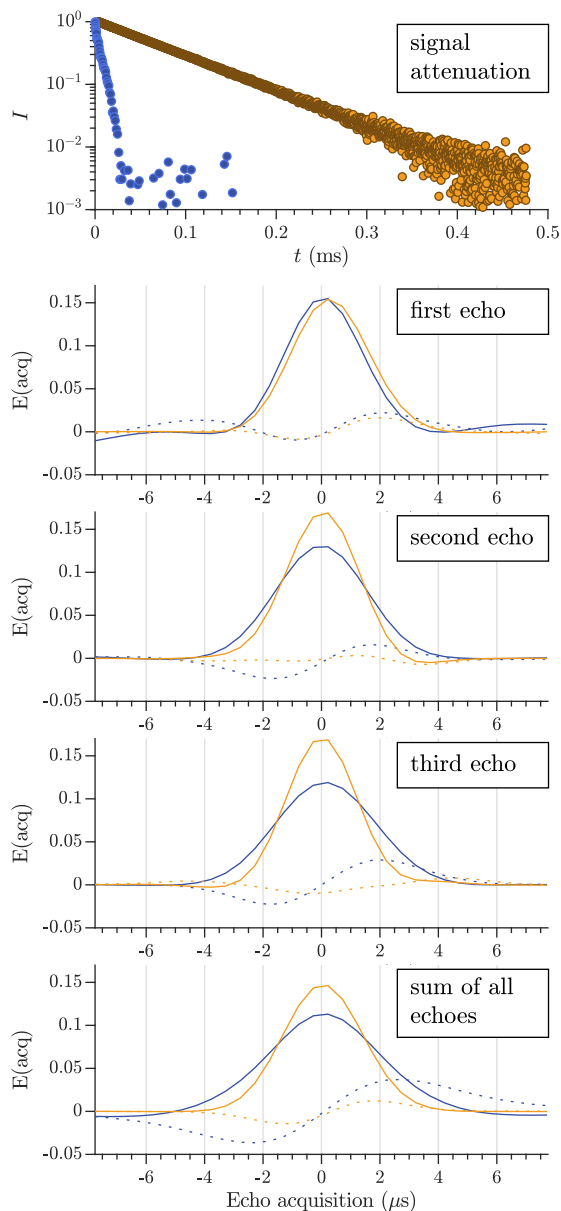


FIG. 5. Comparison of SG-TIETA (blue) and CPMG (orange) attenuation and echo shape for 1-octanol with $2\tau = TE = 98$ ms. Echo shapes show real (solid lines) imaginary (dotted lines) signal normalized by the area under the real signal curve. The echo width of the CPMG decreases with n and stabilizes around $n = 3$, consistent with the approach to asymptotic behavior described in Hürlimann & Griffin⁵⁶. In contrast, the SG-TIETA echo width *increases* and stabilizes around $n = 3$, consistent with the direct echo CTP being preferential to the on-resonance signal.

dence in the observed echo shape behavior and in the consistency of $A_p(n)$ values across different diffusion weightings. Regarding potential applications, SG-TIETA at this g can probe porous media microstructure on micron length scales, i.e., over sub-millisecond timescales. SG-TIETA can also be used to study phenomena associated with other long-range correlations, e.g., poly-

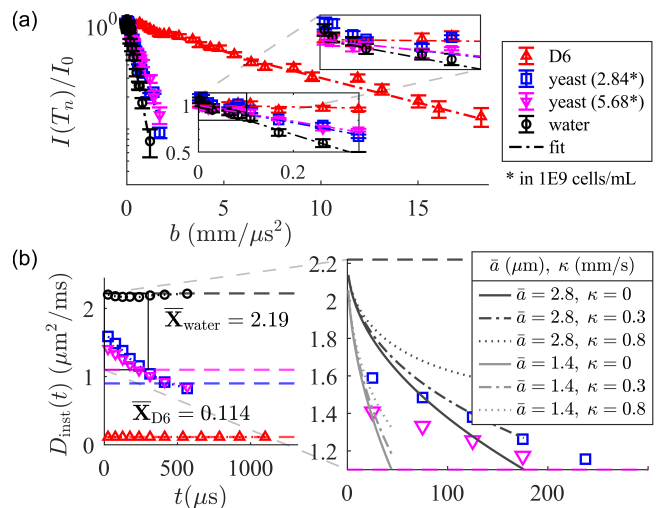


FIG. 6. SG-TIETA decays and inverted \mathbf{X} for D6, yeast, and water. (a) Decays analyzed as described in the text. See SM Section II for fitting procedures. Err. bars = ± 1 SD for, in legend order, 38, 3, 4, 25 repetitions truncated at $n = 34, 17, 17, 15$, respectively. Note erratic early $A_p(n)$ behavior. (b) \mathbf{X} solutions. Inversion parameters were identical to Fig. 3 other than $\Delta t(k)$ for D6. Initial guesses of $D_0 = 2.22$, $D_\infty = \{0.9, 1.1\}$ $\mu\text{m}^2/\text{ms}$ for yeast and $D_0 = D_\infty = 0.114$ $\mu\text{m}^2/\text{ms}$ for D6 were provided. Zoomed plot compares short-time $D_{\text{inst}}(t)$ plotted up to $t < 0.08 \times \tau_D$.

mer dynamics⁶², the glass transition⁶³, and high Péclet fluxes driven by flagella⁶⁴, which likewise exhibit time-dependence in this sub-millisecond range. The methods contained in this Communication may open new avenues of research within DW-NMR.

SUPPLEMENTARY MATERIAL

In the supplementary material, we include sections containing (I) Python code to generate m_j , (II) MATLAB code for the Monte Carlo simulations, fitting procedures, and LLS inversion, (III) a replication of the analysis in Figs. 4 and 6 using SG-TIETA decays for $\tau = 77$ μs , and (IV) additional NMR experimental methodology.

ACKNOWLEDGMENTS

The authors would like to thank Dr. Dan Benjamini and Dr. Michal Komloch for helpful discussions concerning numerical programming and time-based avoidance of unwanted coherence pathways, respectively.

TXC, VW, RR, and PJB were supported by the IRP of the NICHD, NIH. NHW was funded by the NIGMS PRAT Fellowship Award #FI2GM133445-01. PJB, TXC, NHW, and VW conceptualized the work; TXC developed the theory and performed computations; NHW, VW and RR designed and performed experi-

ments; NHW and TXC analyzed data; TXC prepared the manuscript; PJB supervised the project. All authors edited the manuscript.

DATA AVAILABILITY

The data that support the findings of this study are available from the corresponding authors upon reasonable request. The SG-TIETA pulse program and macro can be downloaded from the GitHub repository: <https://github.com/nathanwilliamson/SG-TIETA>.

REFERENCES

- ¹M. Kac, *Amer. Math. Monthly* **73**, 1 (1966).
- ²P. P. Mitra, P. N. Sen, L. M. Schwartz, and P. Le Doussal, *Phys. Rev. Lett.* **68**, 3555 (1992).
- ³P. P. Mitra, P. N. Sen, and L. M. Schwartz, *Phys. Rev. B* **47**, 8565 (1993).
- ⁴P. N. Sen, *Concepts Magn. Reson., Part A* **23A**, 1 (2004).
- ⁵O. Reynaud, *Front. Phys.* **5**, 58 (2017).
- ⁶J. E. Tanner, *J. Chem. Phys.* **69**, 1748 (1978).
- ⁷J. Tanner, *Biophys. J.* **28**, 107 (1979).
- ⁸P. N. Sen, *J. Chem. Phys.* **119**, 9871 (2003).
- ⁹P. N. Sen, *J. Chem. Phys.* **120**, 11965 (2004).
- ¹⁰D. S. Novikov, E. Fieremans, J. H. Jensen, and J. A. Helpert, *Nat. Phys.* **7**, 508 (2011).
- ¹¹R. Mair, P. Sen, M. Hürlimann, S. Patz, D. Cory, and R. Walsworth, *J. Magn. Reson.* **156**, 202 (2002).
- ¹²L. Latour, P. Mitra, R. Kleinberg, and C. Sotak, *J. Magn. Reson.* **101**, 342 (1993).
- ¹³D. S. Novikov, J. H. Jensen, J. A. Helpert, and E. Fieremans, *Proc. Natl. Acad. Sci. U.S.A.* **111**, 5088 (2014).
- ¹⁴E. L. Hahn, *Phys. Rev.* **80**, 580 (1950).
- ¹⁵D. E. Woessner, *J. Chem. Phys.* **67**, 1365 (1963).
- ¹⁶E. O. Stejskal and J. E. Tanner, *J. Chem. Phys.* **42**, 288 (1965).
- ¹⁷C. H. Neuman, *J. Chem. Phys.* **60**, 4508 (1974).
- ¹⁸P. T. Callaghan, A. Coy, D. MacGowan, K. J. Packer, and F. O. Zelaya, *Nature* **351**, 467 (1991).
- ¹⁹W. S. Price, *NMR Studies of Translational Motion: Principles and Applications*, Cambridge Molecular Science (Cambridge University Press, 2009).
- ²⁰J. Keeler, *Understanding NMR spectroscopy* (John Wiley and Sons, Chichester, U.K., 2010).
- ²¹M. Hürlimann, K. Helmer, L. Latour, and C. Sotak, *J. Magn. Reson.* **111**, 169 (1994).
- ²²L. L. Latour, K. Svoboda, P. P. Mitra, and C. H. Sotak, *Proc. Natl. Acad. Sci. U.S.A.* **91**, 1229 (1994).
- ²³P. T. Callaghan and J. Stepišnik, *J. Magn. Reson.* **117**, 118 (1995).
- ²⁴M. Schachter, M. Does, A. Anderson, and J. Gore, *J. Magn. Reson.* **147**, 232 (2000).
- ²⁵E. E. Sigmund, D. S. Novikov, D. Sui, O. Ukpebor, S. Baete, J. S. Babb, K. Liu, T. Feiweier, J. Kwon, K. McGorty, et al., *NMR Biomed.* **27**, 519 (2014).
- ²⁶J. D. Seymour and P. T. Callaghan, *AIChE J.* **43**, 2096 (1997).
- ²⁷A. A. Khrapitchev and P. T. Callaghan, *Phys. Fluids* **15**, 2649 (2003).
- ²⁸D. S. Novikov and V. G. Kiselev, *J. Magn. Reson.* **210**, 141 (2011).
- ²⁹D. C. Douglass and D. W. McCall, *J. Phys. Chem.* **62**, 1102 (1958).
- ³⁰J. Stepišnik, *Physica B+C* **104**, 350 (1981).
- ³¹J. Stepišnik, *Physica B Condens. Matter* **183**, 343 (1993).
- ³²S. Axelrod and P. N. Sen, *J. Chem. Phys.* **114**, 6878 (2001).
- ³³A. L. Sukstanskii and D. A. Yablonskiy, *J. Magn. Reson.* **163**, 236 (2003).
- ³⁴J. Stepišnik, *Physica B Condens. Matter* **270**, 110 (1999).
- ³⁵P. T. Callaghan and J. Stepišnik, in *Advances in Magnetic and Optical Resonance*, edited by W. S. Warren (Academic Press, 1996), vol. 19, pp. 325 – 388.
- ³⁶J. C. Gore, J. Xu, D. C. Colvin, T. E. Yankeelov, E. C. Parsons, and M. D. Does, *NMR Biomed.* **23**, 745 (2010).
- ³⁷L. Ning, K. Setsompop, C.-F. Westin, and Y. Rathi, *Magn. Reson. Med.* **78**, 763 (2017).
- ³⁸H. Y. Carr and E. M. Purcell, *Phys. Rev.* **94**, 630 (1954).
- ³⁹S. Meiboom and D. Gill, *Rev. Sci.* **29**, 688 (1958).
- ⁴⁰L. J. Zielinski and M. D. Hürlimann, *J. Magn. Reson.* **172**, 161 (2005).
- ⁴¹S. Lasič, J. Stepišnik, and A. Mohorič, *J. Magn. Reson.* **182**, 208 (2006).
- ⁴²J. Stepišnik, S. Lasič, A. Mohorič, I. Serša, and A. Sepe, *J. Magn. Reson.* **182**, 195 (2006).
- ⁴³L. J. Zielinski and P. N. Sen, *J. Chem. Phys.* **119**, 1093 (2003).
- ⁴⁴M. Hürlimann, *J. Magn. Reson.* **148**, 367 (2001).
- ⁴⁵A. Ross, M. Czisch, and G. King, *J. Magn. Reson.* **124**, 355 (1997).
- ⁴⁶G. Goelman and M. Prammer, *J. Magn. Reson.* **113**, 11 (1995).
- ⁴⁷Y.-Q. Song, *J. Magn. Reson.* **157**, 82 (2002).
- ⁴⁸J. H. Baltisberger, B. J. Walder, E. G. Keeler, D. C. Kaseman, K. J. Sanders, and P. J. Grandinetti, *J. Chem. Phys.* **136**, 211104 (2012).
- ⁴⁹Y.-Q. Song, *Magn. Reson. Imaging* **23**, 301 (2005).
- ⁵⁰E. E. Sigmund, H. Cho, and Y.-Q. Song, *Concepts Magn. Reson., Part A* **30A**, 358 (2007).
- ⁵¹F. Casanova, B. Blümich, and J. Perlo, *Single-Sided NMR* (Springer, Heidelberg, New York, 2011).
- ⁵²G. Eidmann, R. Savelsberg, P. Blümmler, and B. Blümich, *J. Magn. Reson.* **122**, 104 (1996).
- ⁵³N. H. Williamson, R. Ravin, D. Benjamini, H. Merkle, M. Falgairolle, M. J. O'Donovan, D. Blivis, D. Ide, T. X. Cai, N. S. Ghorashi, et al., *eLife* **8**, e51101 (2019).
- ⁵⁴D. N. Sousa and H. A. Ferreira, *J. Open Source Softw.* **3**, 966 (2018).
- ⁵⁵B. Geil, *Concepts Magn. Reson.* **10**, 299 (1998).
- ⁵⁶M. Hürlimann and D. Griffin, *J. Magn. Reson.* **143**, 120 (2000).
- ⁵⁷K.-J. Suh, Y.-S. Hong, V. D. Skirda, V. I. Volkov, C.-Y. J. Lee, and C.-H. Lee, *Biophys. Chem.* **104**, 121 (2003).
- ⁵⁸J. E. Tanner and E. O. Stejskal, *J. Chem. Phys.* **49**, 1768 (1968).
- ⁵⁹I. Åslund and D. Topgaard, *J. Magn. Reson.* **201**, 250 (2009), ISSN 1090-7807.
- ⁶⁰W. Mazur and A. T. Krzyżak, *Cells* **9**, 2124 (2020).
- ⁶¹G. Karunanithy, R. J. Wheeler, L. R. Tear, N. J. Farrer, S. Faulkner, and A. J. Baldwin, *J. Magn. Reson.* **302**, 1 (2019).
- ⁶²P. T. Callaghan and A. Coy, *Phys. Rev. Lett.* **68**, 3176 (1992).
- ⁶³N. H. Williamson, A. M. Dower, S. L. Codd, A. L. Broadbent, D. Gross, and J. D. Seymour, *Phys. Rev. Lett.* **122**, 068001 (2019).
- ⁶⁴M. B. Short, C. A. Solari, S. Ganguly, T. R. Powers, J. O. Kessler, and R. E. Goldstein, *Proc. Natl. Acad. Sci. U.S.A.* **103**, 8315 (2006).